1   **SARS-CoV-2 and its variants, but not Omicron, induces thymic atrophy and impaired**

2   **T cell development**

3

4

5   Zaigham Abbas Rizvi[1,2], Srikanth Sadhu[1,2], Jyotsna Dandotiya[1,2], Akshay Binyka[1,2], Puja

6   Sharma[3], Virendra Singh[1,2], Vinayaka Das[1,2], Ritika Khatri[4], Rajesh Kumar[4], Sweety Samal[4],

7   Manjula Kalia[3], Amit Awasthi[1,2*]

8

9   [1]Immuno-biology Lab, Infection and Immunology centre, Translational Health Science and

10   Technology Institute, NCR-Biotech Science Cluster, 3rd Milestone, Faridabad-Gurgaon

11   Expressway, Faridabad-121001, Haryana, India

12   [2]Immunology-Core Lab, Translational Health Science and Technology Institute, NCR-

13   Biotech Science Cluster, 3rd Milestone, Faridabad-Gurgaon Expressway, Faridabad-121001,

14   Haryana, India

15   [3]Regional Centre Biotechnology, NCR-Biotech Science Cluster, 3rd Milestone, Faridabad-

16   Gurgaon Expressway, Faridabad-121001, Haryana, India

17   [4]Infection and Immunology centre, Translational Health Science and Technology Institute,

18   NCR-Biotech Science Cluster, 3rd Milestone, Faridabad-Gurgaon Expressway, Faridabad-

19   121001, Haryana, India

20

21

22   ***Corresponding author:**

23   Amit Awasthi, PhD

24   Immuno-biology Laboratory,

25   Translational Health Science & Technology Institute (THSTI)

26   3rd Milestone, Faridabad-Gurgoan Expressway, Faridabad, Haryana, India 121001

27   Email: aawasthi@thsti.res.in

28   Phone: +91-129-287-6482, fax: +91-129-287-6500

29 **Abstract**

30 Pathogenic infections cause thymic atrophy, perturb thymic-T cell development and alter

31 immunological response. Previous studies reported dysregulated T cell function and

32 lymphopenia in coronavirus disease-19 (COVID-19) patients. However, immune-

33 pathological changes, in the thymus, post severe acute respiratory syndrome coronavirus-2

34 (SARS-CoV-2) infection have not been elucidated. Here, we report SARS-CoV-2 infects

35 thymocytes, depletes CD4+CD8+ (double positive; DP) T cell population associated with an

36 increased apoptosis of thymocytes, which leads to severe thymic atrophy in K18-hACE2-Tg

37 mice. CD44+CD25- T cells were found to be enriched in infected thymus, indicating an early

38 arrest in the T cell developmental pathway. Further, Interferon gamma (IFN-γ) was crucial

39 for thymic atrophy, as anti-IFN-γ antibody neutralization rescued the loss of thymic

40 involution. Therapeutic use of remdesivir (prototype anti-viral drug) was also able to rescue

41 thymic atrophy. While Omicron variant of SARS-CoV2 caused marginal thymic atrophy,

42 delta variant of SARS-CoV-2 exhibited most profound thymic atrophy characterized by

43 severely depleted DP T cells. Recently characterized broadly SARS-CoV-2 neutralizing

44 monoclonal antibody P4A2 was able to rescue thymic atrophy and restore thymic

45 developmental pathway of T cells. Together, we provide the first report of SARS-CoV-2

46 associated thymic atrophy resulting from impaired T cell developmental pathway and also

47 explains dysregulated T cell function in COVID-19.

48 **Keywords:** Thymic atrophy, SARS-CoV-2, Delta, Omicron, COVID-19, T cell development,

49 IFNγ, double positive

50

51 SARS-CoV-2 which was first reported in Wuhan, China in Dec, 2019 has so far infected

52 around 5.6% of the total world population with around 1.3% mortality rate as on 29st Feb,

53 2022 (https://covid19.who.int/). While majority of clinical cases report pulmonary

54   pathologies associated with pneumonia and acute respiratory distress syndrome (ARDS),

55   growing number of evidences suggest cardiovascular, gastrointestinal, renal, neurological,

56   endocrinological manifestations of SARS-CoV-2 infection (Chung et al., 2021; Guan et al.,

57   2020; Gupta et al., 2020; Yang and Tu, 2020). Clinical cases of COVID-19 are also

58   characterized by lymphopenia which is defined by T cell lymphodepletion (Tan et al., 2020).

59   In line with this, our clinical data showed a significant depletion of peripheral CD3+ and

60   CD8+ T cells of COVID-19 patients as compared to the healthy control while a decreasing

61   trend was observed for CD4+ T cells (**Fig 1A**). Changes in the thymus post-acute pathogenic

62   infection have been previously shown to cause lymphopenia as thymus is the site of T cell

63   development and maturation (Liu et al., 2014; Luo et al., 2021). Therefore, we speculated that

64   the changes in the thymocytes developmental pathway could be a driving factor for immune

65   dysregulation as seen in COVID-19. For this purpose, we used acute model of SARS-CoV-2

66   infection i.e. hACE2-transgenic (Tg) mice expressing humanized ACE2 receptor driven by

67   epithelial cell cytokeratin-18 (K18) promoter. hACE2-Tg mice has been shown to develop

68   acute SARS-CoV-2 infection following intranasal challenge with the live virus associated

69   with rapid loss in body mass leading to mortality by day 6-8 post infection (McCray et al.,

70   2007; Winkler et al., 2020). Consistent with the published reports, we found that hACE2-Tg

71   mice infected with SARS-CoV-2 (B) develops acute COVID-19 pathology characterized by

72   sharp decline in body mass (**Fig S1A & S1B**), 80% mortality by day 7 and profound presence

73   of lung inflammation and injury as observed by assessing excised lung and hematoxylin and

74   eosin (H&E) stained lung sections by trained pathologist (**Fig S1C- S1G**). In line with this,

75   there was profound localization of N protein in the infected lungs sections as determined by

76   immunohistochemistry (IHC) corresponding to high N gene copy number (by qPCR) (**Fig.**

77   **S1H & S1I**). Characteristic of the active infection, mRNA expression of anti-viral genes

78   which are activated post sensing of viral RNA by toll-like receptors (TLRs) or rig-like

3

Fig. 1
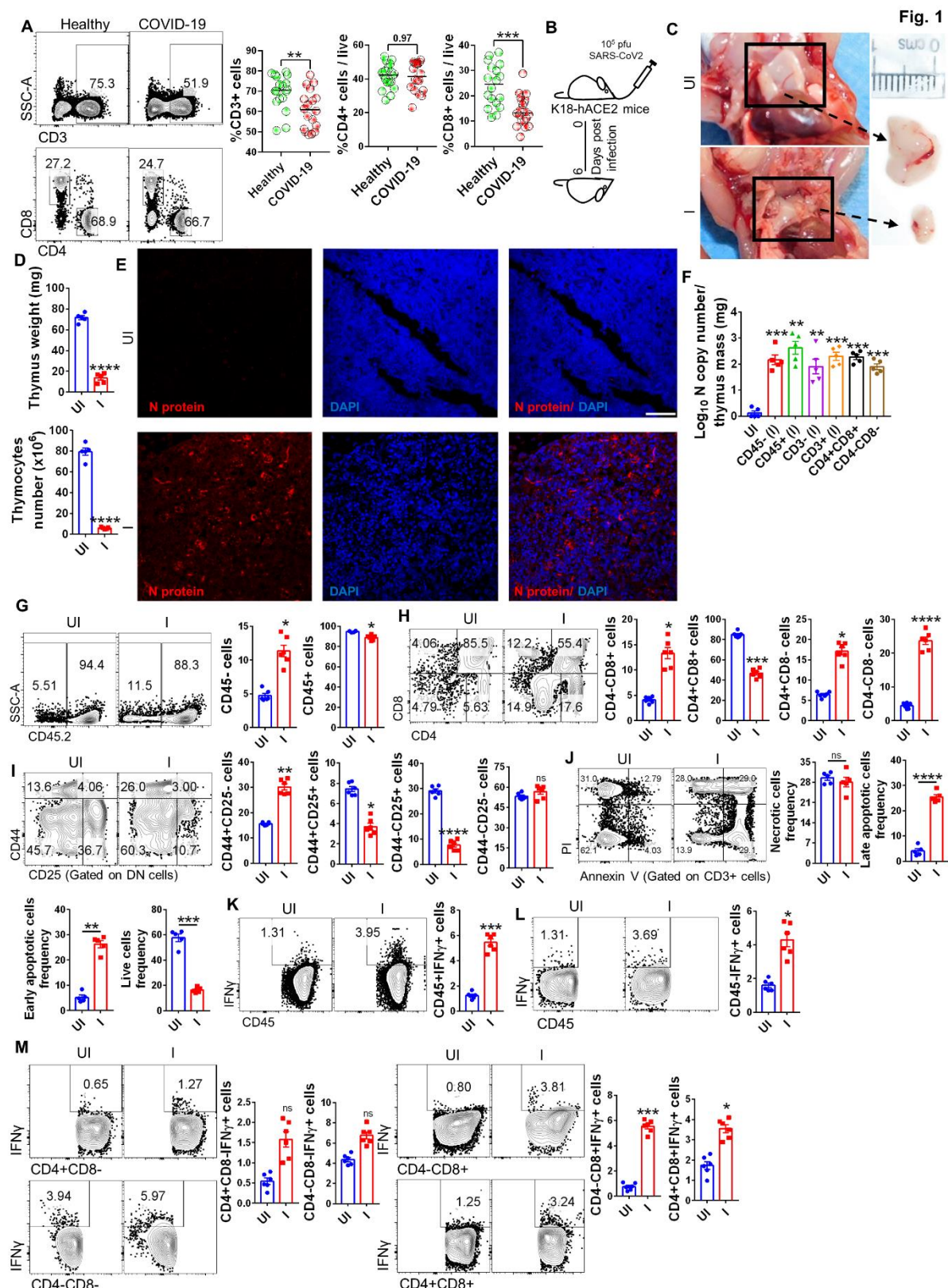
79
80 receptor (RLRs) and activation of stimulator of IFN genes (STING) such as 2'-5'-

81 oligoadenylate synthetase (OAS)-2 and OAS-3, latent RNase (RNaseL), IFN-induced

82 transmembrane (IFITM) protein, adenosine deaminase acting of RNA-1 (ADAR-1)

83 (Schneider et al., 2014) were all significantly increased in infected lung (**Fig. S1J).**

84 Interestingly, the spleen and lymph node size of the infected mice at 6 dpi (peak of acute

85 infection) showed profound involution with decrease in mass and live cell population (**Fig**

86 **S1K-S1O**).

87 Emerging studies now show that lymphopenia is strongly correlated to morbidity and

88 mortality and is associated with more than 50% of the adults and 10% of children infected

89 with SARS-CoV-2 (Adamo et al., 2021; Mathew et al., 2020). Lymphopenia is characterized

90 by a substantial decrease in lymphocyte count and reduction in the frequency of peripheral

91 CD4+ T helper and CD8+ T cytotoxic cells (Mathew et al., 2020). In line with this, we

92 observed significantly reduced frequency as well as cell count of CD45.2+, CD3+, CD4+ and

93 CD8+ lymphocytes in the splenocytes of the infected hACE2-Tg mice at 6 dpi as compared

94 to uninfected mice (UI) (**Fig. S1P-S1Q**). Curiously, there was a 3-4 folds upregulation in the

95 frequency and count of DP cells in the splenocytes, which has been shown to be related to

96 escape of DP cells from the thymus (**Fig. S1P-S1Q**). Lymphopenia seen in acute SARS-

97 CoV-2 infected hACE2-Tg mice strongly pointed to dysregulated T cell development in the

98 thymus. In line with this, the thymus of the infected hACE2-Tg mice at 6 dpi showed

99 profound thymic involution (**Fig 1B & C)** with a 7-8 folds decrease in mass and number of

100 live cells (**Fig. 1D**). Next in order to understand the influence of SARS-CoV-2 infection on

101 the thymic developmental pathway we looked at the virus entry and localization into the

102 thymus. Our immunofluorescence data for SARS-CoV-2 specific anti-N protein localization

103 indicated prominent presence of N protein in the thymocytes of the infected hACE2-Tg (**Fig**

104 **1E)**. This was a surprising finding since no study has so far reported the expression of

105 humanized ACE2 receptor in the thymus of hACE2-Tg mice. Since cellular injury of

106 pulmonary and extra-pulmonary organs is characteristic pathological manifestation of

107 COVID-19 and is often ascribed to the cellular entry and presence of virus, we evaluated the

108 viral load in different compartments of thymocytes i.e. CD45+, CD45-, CD3+, CD3-, DP,

109 DN cells in the sorted population (**Fig. S2A**). Our data shows presence of 2-2.5 log10 N gene

110 copy number/ mg mass in all the compartments of thymocytes, suggesting that virus was able

111 to internalize both in CD45- cells (which comprises of thymic epithelial cells) and CD45+ T

112 cells with equal efficiency (**Fig. 1F**).

113 Next in order to understand whether virus induced thymic involution could result in

114 dysregulation of T cell development we carried out a detailed immunophenotyping for

115 different developmental stages of T cells in the thymus. We found a substantial increase in

116 the frequency of CD45.2- cells, which was accompanied by expansion of CD45.2+ frequency

117 in the infected thymus, however, there was a significant decrease in the cell count of both

118 CD45.2+ and CD45.2- cells, suggesting that the depletion of CD45.2+ cells were higher than

119 that of CD45.2- cells though there was loss of both CD45.2+ and CD45.2- population due to

120 viral infection (**Fig 1G & S2B**). In line with this, we found 2 folds decrease in CD4+CD8+

121 double positive (DP) and ~ 5 folds increase in CD4-CD8- double negative (DN) population

122 with ~ 2-3 folds increase in single positive (SP) CD4+ or CD8+ cells indicating a profound

123 dysregulation of T cell developmental pathway in infected thymus (**Fig 1H**). Since

124 dysregulated ratio of DP/DN was observed in thymus of infected mice, we made an attempt

125 to understand at which developmental stage of triple negative (TN) population int the thymus

126 is getting affected. Thymic development of TN occurs in 4 distinct stages viz CD44+CD25-

127 (DN1), CD44+CD25+ (DN2), CD44-CD25+ (DN3) and CD44-CD25- (DN4) (Haynes et al.,

128 1999; Liu et al., 2014). We found that thymus of the infected mice showed accumulated

129 frequency for DN1 stage while a decrease in DN2 and DN3 percent frequency was observed

130 for infected samples, suggesting an arrest at the early stage of T cell developmental pathway

131 (**Fig 1I**). We found ~ 4-6 folds increase in early and late apoptotic cells CD3+ thymocytes in

132 infected as compared to the uninfected control (**Fig 1J**). Similar trends in the induction of

133 early and late apoptosis was found on CD45+ thymocytes, however CD45- thymocytes

134 showed lesser frequency of apoptotic cells suggesting that CD3+ thymocytes are the major

135 depleted population during SARS-CoV-2 infection in mice (**Fig S2C & S2D).** When time

136 kinetics of infection pathology was studied to understand the early or late phase induction of

137 thymic atrophy, we found that the degree of thymic atrophy was directly proportional to the

138 severity of coronavirus disease-19 (COVID-19) with profound thymic atrophy at day 6 (but

139 not day 3: I_3 post challenge) (**Fig S2E-S2J).**

140 Several mechanisms have been shown to influence thymic atrophy for pathogenic infection

141 such as NK cells activation, increased levels of glucocorticoids as well as heightened IFN-γ

142 secretion by the thymocytes. Previously studies have shown that pathogenic infections causes

143 thymic atrophy associated with apoptosis of thymocytes which could be mediated by IFN-γ

144 induced tissue injury (Barreira-Silva et al., 2021; Liu et al., 2014; Savino, 2006). Our data

145 shows that SARS-CoV-2 infection results in profound elevation (~5 folds) of IFN-γ by

146 CD45+ cells and to lesser extend (~2 fold) by CD45- cells (**Fig 1K & L**). Moreover, SP

147 CD8+ cells were found to be the major contributors of IFN-γ production in the thymus with ~

148 6 fold upregulation during infection (**Fig 1M)** which could be one of the driving factors for

149 thymic atrophy as has been earlier reported (Liu et al., 2014). Other pro-inflammatory cytokines

150 such as Granzyme B (GzB), IL-4 and IL-17A was not found to be significantly altered, however

151 interestingly, Perforin-1 (Prf-1) was found to be significantly up-regulated upon infection (**Fig. S2K-**

152 **S2N)**. Together, we show that SARS-CoV-2 infection in hACE2-Tg mice results in thymic

153 atrophy. Thymic atrophy was characterized by loss of DP population probably due to

154 apoptosis and heightened IFN-γ which could be due to the persistence of virus in the thymus.

155 IFN-γ, produced by both innate and adaptive arms of the immune system, has been earlier

156 shown to be crucial mediator of inflammation and tissue injury during viral infections.

Fig. 2
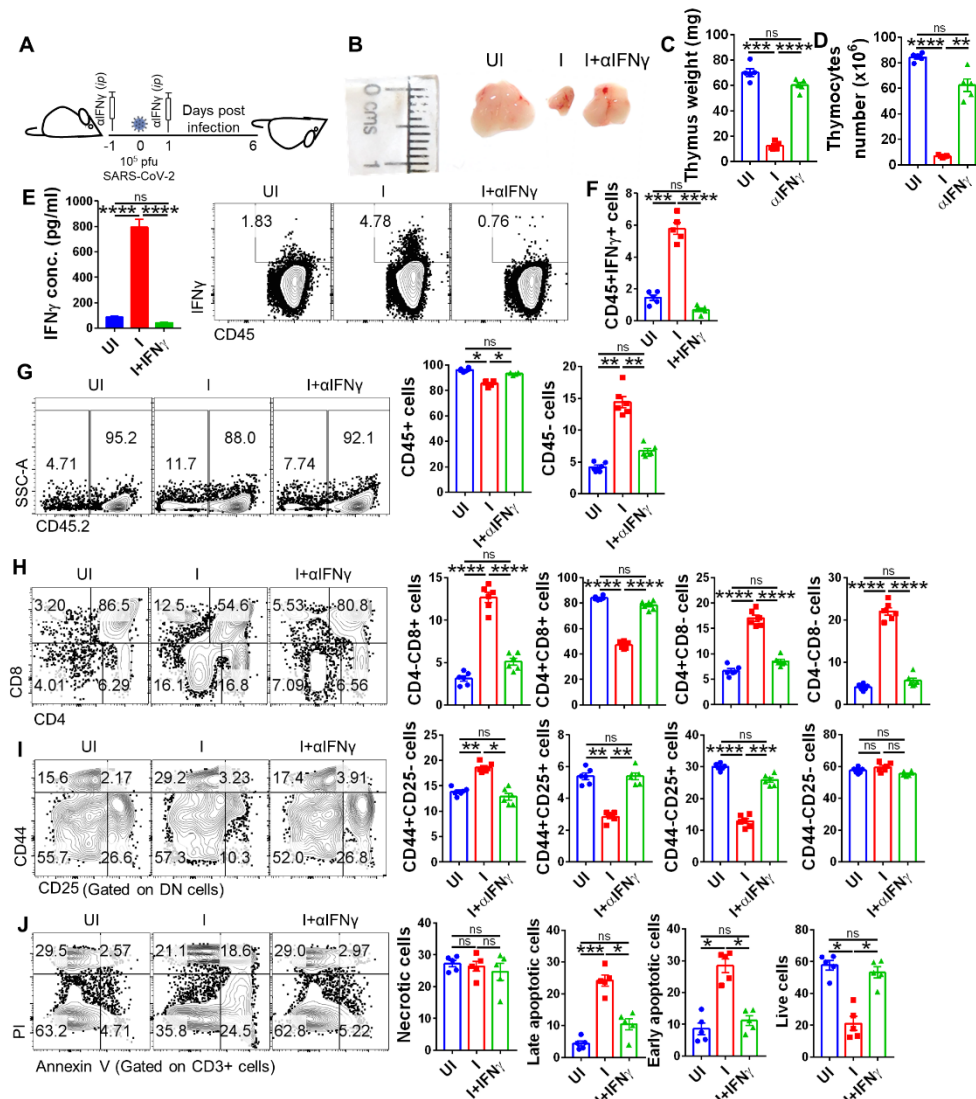
Moreover, IFN-γ is critical in the induction of activation induced cell death (AICD) in T cells (Refaeli et al., 2002). Elevated levels of IFN-γ was one of the key component of cytokine release syndrome in human and animal model (Moore and June, 2020). In fact, our data indicate that a heightened IFN-γ levels in SARS-CoV2-infected hamster and K18-ACE2-Tg mice. In thymus, IFN-γ has been implicated in apoptosis of thymocytes resulting in tissue injury and thymic atrophy (Elfaki et al., 2021; Liu et al., 2014). One previous study have shown that thymic atrophy caused due to influenza A virus could be alleviated by neutralizing IFN-γ (Liu et al., 2021). Since many aspects of pathogenesis and immunological response of influenza A virus and SARS-CoV-2 bear similarity, we speculated that IFN-γ could be one the key mediators of thymic atrophy for SARS-CoV-2 (Flerlage et al., 2021),

8

168   and thus neutralize IFN-γ functions by using anti- IFN-γ neutralizing antibody. Anti-mouse

169   IFN-γ neutralization was done one day prior and one day post SARS-CoV-2 infection in

170   hACE2-Tg mice in order to neutralize the effector functions of IFN-γ induced upon SARS-

171   CoV-2 infection **(Fig. 2A)**. There was marginal protection in the body weight loss (**Fig S3A**)

172   but no significant decrease in lung viral load in IFN-γ neutralized animals (**Fig S3B).**

173   However, thymus of the animals receiving anti-IFN-γ antibody neutralization (I+IFN-γ)

174   showed little or no signs of thymic involution in terms of size, mass and number when

175   compared to the thymus from uninfected mice (**Fig 2B-D**). This corroborated with the

176   decreased level of IFN-γ in animals receiving neutralizing antibody (**Fig. 2E-F**). In line with

177   the rescue of thymus size, the percentage frequency of CD45.2+/- cells were restored to

178   normal levels as seen in uninfected control thymus (**Fig 2G**). Moreover, the percentage

179   frequency of DP and DN cells along with the percentage of DN1-DN4 population was also

180   found to recover to their corresponding uninfected percentage frequency (**Fig 2H-I**). Finally,

181   we showed that neutralization of IFN-γ effectively blunted the apoptosis of thymocytes, thus

182   validating that the important and sufficient mediator of thymic atrophy in SARS-CoV-2

183   hACE2-Tg mice is IFN-γ **(Fig. 2J).** Since, SARS-CoV-2 in hACE2-Tg mice resulted in

184   profound IFN-γ response, we asked whether IFN-γ induced tissue injury could also occur in

185   C57BL/6 (WT) mice infected with SARS-CoV-2 without necessitating hACE2 receptor

186   dependent virus entry. Remarkably, SARS-CoV-2 infected WT mice did not show any signs

187   of pulmonary pathology or thymic involution as seen in hACE2 mice (**Fig S3C-S3L).**

188   Together, our findings show that elevated IFN-γ secretion in SARS-CoV-2 infected hACE2-

189   Tg mice leads to tissue inflammation and injury, thereby causing IFN-γ dependent thymic

190   atrophy.

191   In the beginning we described that SARS-CoV-2 infection through intranasal route results in

192   virus entry and localization in the thymus. Presence of virus or viral factors have been shown

193   to activate TLR3, TLR7 and TLR8 and RLR which leads to induction of anti-viral genes and

194   cytokines characterized by heightened IFN-γ response (Bonifacius et al., 2021; Moore and June,

195   2020). This would mean that the use of anti-viral drugs which could reduce the viral burden

196   and reduce viral antigens would also effectively reduce the inflammatory IFN-γ production and

197   hence thymic atrophy. To test this, we used remdesivir (RDV, a prototypic anti-viral drug)

198   which has been shown to have significant efficacy against SARS-CoV-2 infection in clinical

199   cases (Beigel et al., 2020; Wang et al., 2020). Challenged animals receiving remdesivir

200   (I+RDV) treatment significantly reduced lung viral loads and rescued mice from SARS-

201   CoV2 induced pathologies (**Fig 3A, S3M-S3N**). In line with this, RDV treatment in SARS-

202   CoV2 infected mice significantly reduced thymic involution with size, mass and number of

203   live thymocytes restored (approx.) to that of the uninfected animals **(Fig 3B-D)**.

204   Corresponding to this protection, there was profound reduction in the viral load throughout

205   the thymus as assessed by immuno-fluorescence microscopy and qPCR (**Fig 3E-3F**). In

206   addition, animals receiving RDV treatment resulted in alleviation of thymic atrophy immune

207   profile and rescued the normal developmental pathway of thymocytes with restored levels of

208   CD45+/-, DP, DN cells (**Fig 3G-H).** In line with this, the developmental stages of DN

209   population from DN1-DN4 was restored back to their corresponding uninfected profiles **(Fig.**

210   **3I**). Next, we also evaluated the levels of IFN-γ and thymocytes apoptosis as it was important

211   to understand whether RDV mediated rescue of thymic atrophy was operational through

212   clearance of viral load from the thymus or it also resulted in blunted the inflammatory

213   response and related thymic injury. IFN-γ response of CD45+ cells were reduced following

214   RDV treatment and it also resulted in reduced percent frequency of thymocytes entering

215   apoptosis which was expected as viral load and inflammation were earlier shown to be the

216   driving factors for apoptosis of thymocytes **(Fig. 3J-L)**. Together, we establish that

217   reminiscent of IFN-γ, use of RDV (anti-viral drug) could effectively reduce the viral burden

Fig. 3
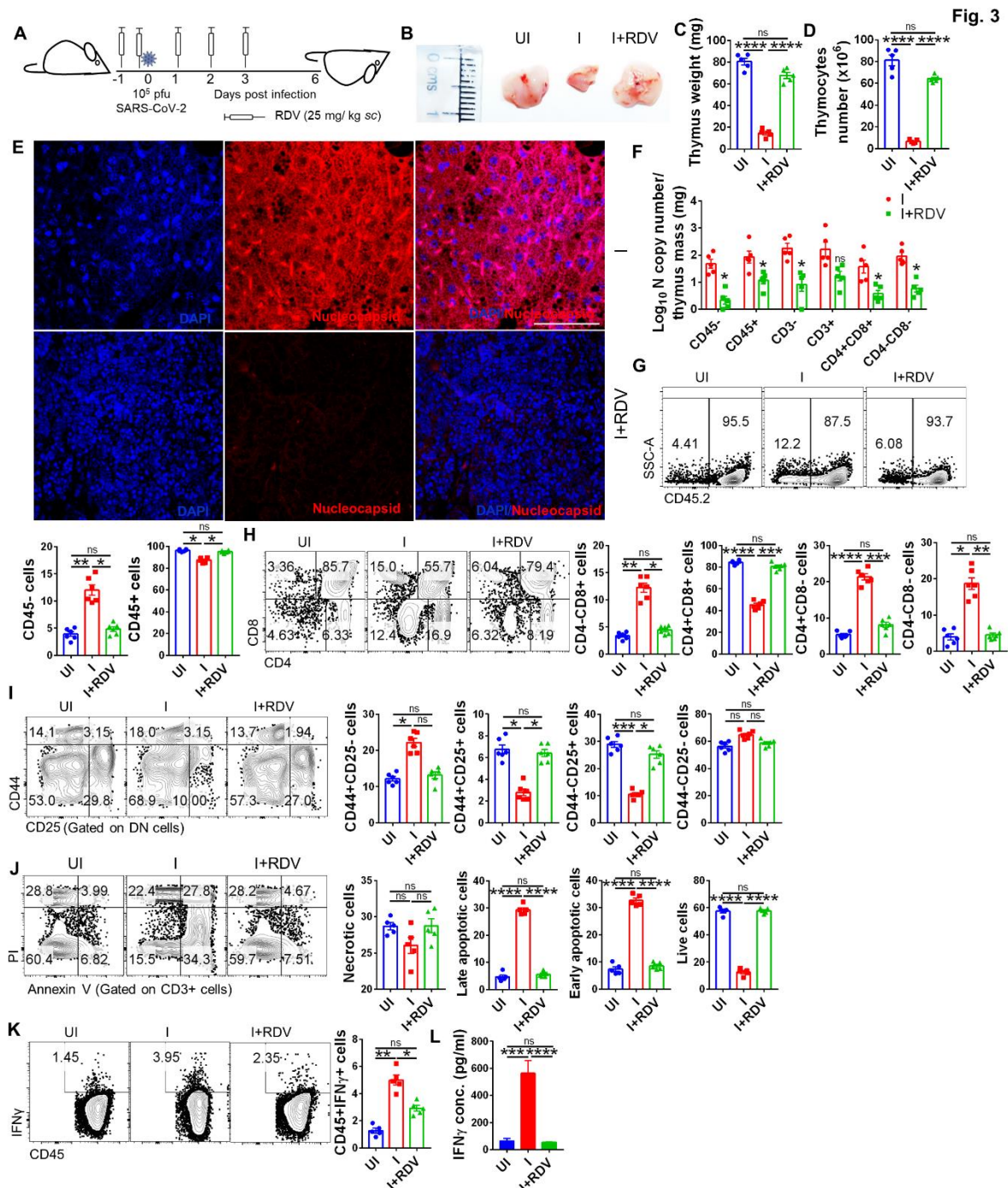
218
219   could rescue the thymic atrophy induced by SARS-CoV-2 infection.

220   In contrast to hACE2-Tg mice, golden Syrian hamster model mimics mild to moderate

221   coronavirus disease-19 (COVID-19) as observed in majority of clinical cases (Chan et al.,

222   2020). In addition, we had earlier shown that the pulmonary pathology of coronavirus

223   disease-19 (COVID-19) following SARS-CoV-2 infection in hamster peaks at 2-4 days post

224   infection (dpi) with highest lung viral load, and starts to decline by 5-6 dpi with

225   comparatively lower viral load and pulmonary pathology on 7 dpi (Rizvi et al., 2022).

226   Induction of thymic atrophy was evaluated at early and late phase in infected hamsters i.e. 4

227   and 7 dpi (**Fig S3O**). Though there was no significant difference in the size and mass of the

228   excised thymus at 4 and 7 dpi as compared to that of 0 dpi thymus (**Fig S3P & S3Q**), the

229   number of live thymocytes as measured by trypan blue exclusion dye was significantly lower

230   at 4 dpi (peak of infection) as compared to 0 dpi (uninfected) or 7 dpi (recovery phase of

231   infection), suggesting signs of thymic injury at the peak of infection (**Fig S3R**). Thymus of

232   the 4 dpi hamsters showed 100-500 copy number of viral gene N/ mg of thymus indicating

233   thymic entry of SARS-CoV-2 (**Fig S3S**). We used anti-mouse CD4 (GK 1.5, cross reactive to

234   hamster CD4) and anti-rat CD8 (cross reactive to hamster CD8) both having cross-reactivity

235   with respective CD markers of hamster to study the development of T cells in thymus.

236   Remarkably, we found 12-15% decrease in the DP cells at 4 dpi and 3-5% decrease in DN at

237   7 dpi as compared to the 0 dpi thymus DP cells. Similar dysregulated ratios were observed

238   for SP CD4 and CD8 cells at 4 dpi. There was a sharp increase in DN cells at 4 dpi with

239   approx. 2-fold increase as compared to 0 dpi thymus suggestive of dysregulated T cell

240   development (**Fig S3T**). In line with this, we found 3-4 folds increase in early and late

241   apoptotic cells at 4 dpi thymus accompanied with approx. 3 folds increase in thymic IFN-γ

242   levels as compared to uninfected control (**Fig S3U & S3V**). Together, our findings show that

243   acute COVID-19, but not moderate COVID-19 leads to severe thymic atrophy.

244   The original Wuhan strain of SARS-CoV-2 (2019-nCoV) which caused first wave of

245   pandemic in 2020 acquired continuous and considerable mutations in genetic material leading

246   to antigenically different mutations which have been so far characterized into variants of

247   concern (VoC), these VoCs lead to subsequent waves of pandemics across the globe or at

248   different regions of the globe at different time points (Geers et al., 2021). One such major

249   VoC reported for SARS-CoV-2 was beta variant (B.1.351) that was first detected in South

Fig. 4

Cont. fig. 4

251
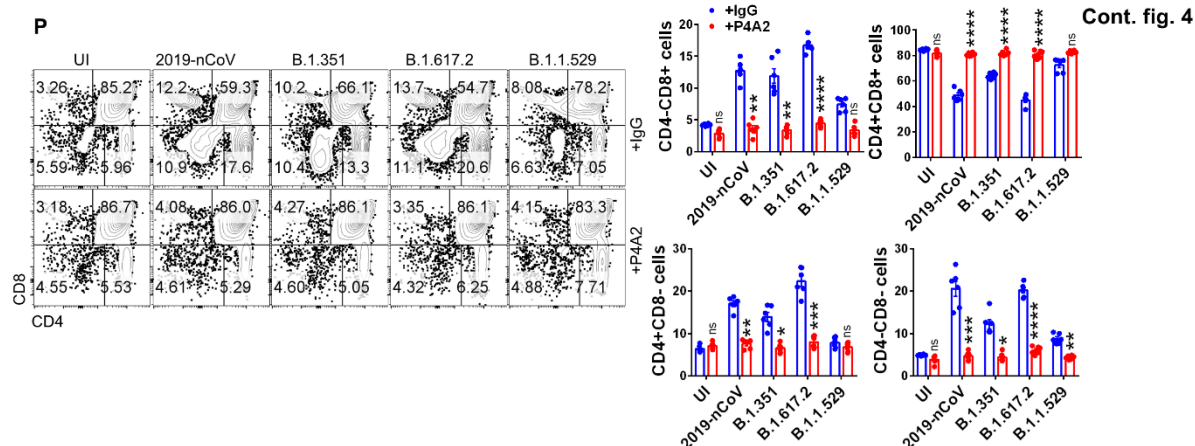
252 Africa with a large number of mutations in the spike region. The two other notable VoC

253 appeared were Delta variant (B.1.617.2) first detected in India in late 2020 and recently

254 reported omicron variant (B.1.1.529) (McCallum et al., 2021, 2022). While both B.1.617.2

255 and B.1.1.529 have been shown to accumulate large amount of mutations in spike and

256 receptor binding domain (RBD) and evade immune response, but only B.1.617.2 but not

257 B.1.1.529 have been shown to cause severe COVID19 in hACE2-Tg animal model

258 (Halfmann et al., 2022). Since mutations reported in the VoC have been shown to evade

259 immune response we became interested to investigate the effect of VoC challenge B.1.351,

260 B.1.617.2 and B.1.1.529 on the induction of thymic atrophy (**Fig 4A**). Consistent with the

261 previously published reports, mice infected with variants except omicron showed rapid

262 decrease in body mass and with presence of high N-gene copy number (**Fig S4A-S4B**). Our

263 data demonstrate a most profound thymic atrophy in animals challenged with B.1.617.2

264 variant which closely mimicked the degree of thymic dysregulation of 2019-nCoV both in

265 terms of involution of size, mass and thymocytes number. Interestingly, animals challenged

266 with B.1.1.529 showed marginal thymic atrophy when compared to the original 2019-nCoV

267 strain in line with the lower lung viral load **(Fig. 4B-D)**. Consistent with the thymic atrophy

268 we found significant VoC viral load in all the cellular compartment of thymus which was

269 relatively lower for B.1.1.529 variant (**Fig 4E**). The profile of developing thymocytes as well

270 as levels of IFN-γ secretion followed the pattern of infectivity with B.1.617.2 showing the

14

271   highest while B.1.1.529 variant showing lowest dysregulation respectively when compared

272   uninfected control (**Fig 4F-4J & S4C-S4G**). Among the other pro-inflammatory cytokines

273   only Prf-1 was found to be significantly elevated across VoC in CD4/CD8 thymocytes sub-

274   sets (**Fig S4H-S4K).**

275   We previously demonstrated that the use of anti-viral drug RDV as an effective prophylactic

276   treatment for rescuing thymic atrophy. We further investigated the therapeutic efficacy of

277   P4A2, a murine monoclonal antibody broadly potent against VoC including Omicron by

278   binding to the receptor binding motif (RBM) of SARS-CoV-2 RBD protein (Kumar et al.,

279   2022). Monoclonal antibodies have previously shown to be effective in neutralizing SARS-

280   CoV-2 in clinical settings and have the advantage of being administered as therapeutic dose

281   post challenge even to immuno-compromised individuals (Brouwer et al., 2020). We found

282   effective neutralization of VoC and alleviation of thymic involution in mice receiving P4A2

283   antibody (**Fig 4K-N**). Likewise, the profile of the developing thymocytes along with the

284   masking of IFN-γ secretion was also seen with the therapeutic dosing of P4A2 against all the

285   VoC studied (**Fig 4O-4P**). Together, we show that the therapeutic dose of P4A2 antibody was

286   effective and sufficient to neutralize VoC challenge and restore the thymic atrophy condition

287   induced by SARS-CoV2 challenge.

288   In summary, we present the first report of thymic atrophy induced by SARS-CoV-2 infection

289   in both moderate and acute COVID19 model. Lymphopenia and immune dysregulation is a

290   common feature of many pathogenic infection including influenza A and is influenced by the

291   changes in the thymus. Moreover, thymus is the primary lymphoid organ and is central to the

292   immune hemostasis. Through our study, we found that lymphopenia associated with SARS-

293   CoV-2 infection could be attributed to thymic dysregulation and thymic atrophy. Since

294   lymphopenia is known to persist long after COVID19 infection in clinical cases, we believe

295   that thymic atrophy could be one of the important contributors of lymphopenia and may

296   contribute to the alteration in peripheral T cell receptor repertoir. These findings may provide

297   a paradigm change in our understanding of how immune-response (especially T cell

298   response) is modulated during COVID-19 and may provide novel mechanism for designing

299   vaccine candidates since thymic atrophy had been shown to result in loss of TCR repertoire.

Acknowledgments

Author Contributions

312   Conceived, designed and supervised the study: AA; Designed and performed the

313   experiments: ZAR; ABSL3 experiment: ZAR, SS, JD; FACS: ZAR, SS, JD; qPCR: ZAR;

314   ELISA: ZAR; Floursecence microscopy: PS, MK; Antibody P4A2: RK; Analyzed the data:

315   ZAR; Contributed reagents/materials/analysis tools: AA; Wrote the manuscript: ZAR, AA.

Declaration of Interests

317   The authors declare no conflict of interest.

Data availability statement

319 All data needed to evaluate the conclusions in the paper are present in the paper and/or the

320 Supplementary Materials

321 **Competing Interests**

322 The authors declare no competing interest.

323 **Figure legends**

324 **Figure 1. Immuno-pathology of thymus of SARS-CoV-2 infected animals.** (A)

325 Immunophenotyping of COVID-19 patients compared to healthy controls (n=18 each). Each

326 dot SSC-A vs CD3, CD4 vs CD8 represents the %frequency of respective cell types per total

327 live cells in PBMCs of an individual subject. Bars represent median values for % CD3

328 cells/live % CD4 cells/live % CD8 cells/live. **(I-M)** hACE2-Tg mice intranasally (I) infected

329 with 10^5 pfu SARS-CoV-2 were euthanized at the time points indicated and immuno-

330 pathological changes in the thymus was studied as compared to the uninfected (UI) control.

331 (B) Schematic representation of hACE2-Tg transgenic mice study. The animals were

332 sacrificed on day 6 or on the day they become moribund or otherwise indicated. (C)

333 Representative image of excised thymus along with thymus (D) weight and number. (E)

334 Immunofluorescence microscopy image of thymus section showing SARS-CoV-2 specific N

335 protein (red color), DAPI stain (blue color) and overlay image (DAPI+N protein) acquired at

336 60X magnification. (F) bar graph showing mean $\pm$ SEM of N gene copy for sorted

337 populations of thymus. Representative FACS dot plot and its corresponding bar graph

338 showing percentage frequency mean $\pm$ SEM showing (G) SSC-A vs CD45.2 (H) CD4 vs

339 CD8 gated on CD45.2+ cells (I) CD44 vs CD25 gated on DN cells (J) PI vs Annexin V gated

340 on CD3+ cells (K) IFN-γ vs CD45+ (L) IFN-γ vs CD45- and (M) IFN-γ vs different

341 CD4/CD8 sub-populations in the thymus. (D-F) n=5; (B-C, G-M) n=6. Non-parametric t-test

342 using Mann-Whitney test. *P < 0.05, **P < 0.01, ***P < 0.001, ****P < 0.0001.

343 **Figure 2. Effect of IFN-γ neutralization on thymic atrophy in SARS-CoV-2 infected**

344 **hACE2-Tg mice.** Neutralizing monoclonal antibody against IFN-γ was used to understand

345 the response of IFN-γ neutralization on thymic atrophy in infected mice. (A) schematic

346 representation indicating schedule for anti-IFN-γ antibody injection. (B) Representative

347 images of excised thymus. (C & D) Bar graph showing mean $\pm$ standard error mean (SEM) of

348 thymus wight (mg) and live thymocytes. (E) BALF IFN-γ quantitation by ELISA.

349 Representative FACS dot plot and its corresponding bar graph showing percentage frequency

350 mean $\pm$ SEM showing (F) IFN-γ vs CD45 (G) SSC-A vs CD45.2 (H) CD4 vs CD8 gated on

351 CD45.2+ cells (I) CD44 vs CD25 gated on DN cells (J) PI vs Annexin V gated on CD3+ cells

352 in the thymus. (C-E) n=5; (A-B, E-I) n=6. One way-Anova using non-parametric Kruskal-

353 Wallis test for multiple comparison. $*P < 0.05$, $**P < 0.01$, $***P < 0.001$, $****P < 0.0001$.

354 **Figure 3. Effect of remdesivir treatment on thymic atrophy in SARS-CoV-2 infected**

355 **hACE2-Tg mice.** Protective efficacy of remdesivir (RDV), used as a prototypic anti-viral

356 drug, against induction of thymic atrophy upon SARS-CoV-2 infection in hACE2-Tg mice.

357 (A) schematic representation showing treatment regime and dose of remdesivir given to

358 SARS-CoV-2 infected mice. (B) Representative images of excised thymus. (C & D) Thymus

359 weight and number shown by bar graph indicating mean $\pm$ standard error mean (SEM). (E)

360 Images of immunofluorescence microscopy of thymus section showing SARS-CoV-2

361 specific N protein (red color), DAPI stain (blue color) and overlay image (DAPI+N protein)

362 acquired at 60X magnification. (F) N gene copy number for sorted thymic populations shown

363 by bar graph mean $\pm$ SEM. FACS representative dot plot and its respective bar graph

364 showing percentage frequency mean $\pm$ SEM indicating (G) SSC-A vs CD45.2 (H) CD4 vs

365 CD8 gated on CD45.2+ cells (I) CD44 vs CD25 gated on DN cells (J) PI vs Annexin V gated

366 on CD3+ cells (K) IFN-γ vs CD45 in the thymus. (L) Evaluation of IFN-γ from BALF

367 samples by ELISA. (C-F, L) n=5; (A-B, G-K) n=6. One way-Anova using non-parametric

18

368   Kruskal-Wallis test for multiple comparison. *P < 0.05, **P < 0.01, ***P < 0.001, ****P <

369   0.0001.

370   **Figure 4. Immuno-pathological changes in thymus infected by SARS-CoV-2 variants**

371   **and its recovery by broadly SARS-CoV-2 neutralizing monoclonal antibody P4A2.**

372   Induction of thymic atrophy in hACE2-Tg mice challenged with SARS-CoV-2 variants such

373   as beta variant (B.1.315), delta variant (B.1.617.2) and omicron variant (B.1.1.529) was

374   studied by intranasal infection 10^5 pfu/ mice followed by euthanization 6 days post infection

375   or on the day when animals became moribund. (A) schematic diagram for VoC challenged

376   hACE2-Tg mice. (B) Representative images of excised thymus. (C & D) Mean bar graph $\pm$

377   SEM showing thymus wight (mg) and live thymocytes. (E) N gene copy number for sorted

378   thymic populations shown by bar graph mean $\pm$ SEM. FACS representative dot plot and its

379   respective bar graph showing percentage frequency mean $\pm$ SEM indicating (F) SSC-A vs

380   CD45.2 (G) CD4 vs CD8 gated on CD45.2+ cells (H) PI vs Annexin V gated on CD3+ cells

381   (I) IFN-γ vs CD45 for UI and VoCs in the thymus. (J-O) Therapeutic efficacy of P4A2

382   broadly SARS-CoV-2 neutralizing antibody in protecting against thymic atrophy by SARS-

383   CoV-2 variants. (J) IFN-γ ELISA from BALF samples. (K) Scheme for VoC challenge in

384   presence or absence of P4A3. (L) Representative image of excised thymus along with (M)

385   thymus weight and (N) number. Representative FACS dot plot and its corresponding bar

386   graph showing percentage frequency mean $\pm$ SEM for VoC thymus in presence or absence of

387   P4A2 (O) SSC-A vs CD45.2 (P) CD4 vs CD8 gated on CD45.2+ cells in the thymus. (C-E, J,

388   L-N) n=5; (A-B, F-I, K-L, O-P) n=6. (C-I) One way-Anova (L-O) Two-way Anova using

389   non-parametric Kruskal-Wallis test for multiple comparison. *P < 0.05, **P < 0.01, ***P <

390   0.001, ****P < 0.0001.

391

Fig. 1

Fig. 2

Fig. 3

Fig. 4

P

Cont. fig. 4